PV Micro-Inverter Topology Using LLC Resonant Converter

Hiroki Watanabe [1], Jun-ichi Itoh [1,*], Naoki Koike [2] and Shinichiro Nagai [2]

[1] Department of Electrical, Electronics and Information Engineering, Nagaoka University of Technology, Kamitomiokamachi, Nagaoka, Niigata 940-2137, Japan

[2] Pony Electric Co., Ltd., Kitasaiwai, Yokohama, Kanagawa 220-0004, Japan

* Correspondence: itoh@vos.nagaokaut.ac.jp; Tel.: +81-258-47-9561

Abstract: In this paper, a DC–single-phase AC power converter with an LLC resonant converter is presented for a photovoltaic (PV) micro-inverter application. This application requires the leakage current suppression capability. Therefore, an isolated power converter is usually combined for DC/AC systems. The LLC resonant converter is the one of the isolated power converter topologies, and it has good performance for conversion efficiency with easy control. On the other hand, a double-line frequency power ripple has to be compensated for in order to improve the performance of the maximum power point tracking (MPPT). Therefore, a bulky electrolytic capacitor is usually necessary for the power converter. However, the electrolytic capacitor may limit the lifetime of the micro-inverter. This paper introduces the PV micro-inverter with a LLC resonant converter. In addition, the active power decoupling circuit is applied in order to compensate the double-line frequency power ripple by the small capacitor in order to eliminate the electrolytic capacitor. Finally, the transformer design is considered in order to reduce the transformer losses. As a result, the conversion efficiency of the LLC converter is improved by 1% when the litz wire has many strands.

Keywords: PV micro-inverter; LLC converter; high switching frequency; transformer loss

---

1. Introduction

Recently, photovoltaic systems (PVs) are actively researched as a sustainable power solution due to their attractive characteristics such as flexibility, high system efficiency, and low manufacturing cost. In order to enhance the utilization of PVs, the generative power optimization by MPPT is necessary. However, the decrease of the generative power due to the shade is a problem for PVs with the typical centralized power conversion system (PCS). In order to solve this problem, AC module systems using micro-inverters are attractive in comparison with large capacity inverters [1–4]. This is because the micro-inverters optimize the generation power at each PV module. Note that the micro-inverters consist of the DC/AC converter and the isolated DC/DC converter because the leakage current due to the stray capacitance of the PV panel should be avoided for safety reasons and for easy installation. In this case, a flyback converter or push-pull converter is often chosen because these circuits have some advantages, e.g., a low number of components.

On the other hand, the LLC resonant converter is also one choice for the isolated DC/DC converter, because it has good performance to reduce the switching losses utilizing Zero Voltage Switching (ZVS) and Zero Current Switching (ZCS) by series resonance [4–9]. In particular, the parasitic capacitor is discharged before being turned on by the negative current. On the other hand, each drain current approximately becomes zero when each switch is turned-off, owing to the sinusoidal resonance current. That means the turn-on and the turn-off switching losses are drastically reduced by the ZVS and ZVS operation. In addition, the volume of the transformer is drastically reduced owing to the high

switching frequency operation being same as the push-pull converter or flyback converter. Note that in the single-phase AC grid systems, a double-line frequency ripple occurs in the input current due to the single-phase AC grid, and the current ripple decays the performance of the MPPT because the PV generative power becomes unstable. Therefore, the bulky electrolytic capacitor is usually installed on the DC side. However, the bulky electrolytic capacitor may limit the lifetime of the power converter because the micro-inverter has to operate on the high environmental temperature condition although the lifetime of the electrolytic capacitor depends on the Arrhenius law. In order to solve this problem, the active power decoupling topologies have been studied to compensate the current ripple [10,11]. These topologies utilize the small capacitor such as a firm or ceramic capacitor for the power decoupling. Thus, an electrolytic capacitor is not necessary.

In this paper, a PV micro-inverter using an LLC converter is presented. In addition, the active power decoupling circuit based on the boost converter is combined with the micro-inverter in order to eliminate the bulky electrolytic capacitor in order to improve the reliability. Finally, the conversion efficiency of the LLC resonant converter is evaluated using two type litz wire in order to reduce the skin effect due to the high switching frequency operation. The contribution of this paper is that the influence of the number of strands to the conversion efficiency is evaluated in order to improve the conversion efficiency of the high frequency power converter. A lot of papers have only considered the transformer loss or the inductor loss [12], and the relationship between the number of strands and the conversion efficiency is not clarified.

2. Circuit Configuration

Figure 1 shows the PV power generative system. Typically, the centralized inverter, as shown in Figure 1a, is employed, and the generative DC power is translated to single-phase AC. In this system, each generative power of the PV modules is regulated by the single inverter with a large power rating. On the other hand, the micro-inverter as shown in Figure 1b is integrated to the PV modules, and each power converter is connected to the single-phase grid directly. Therefore, it is possible to optimize the generative power at each of the PV modules.
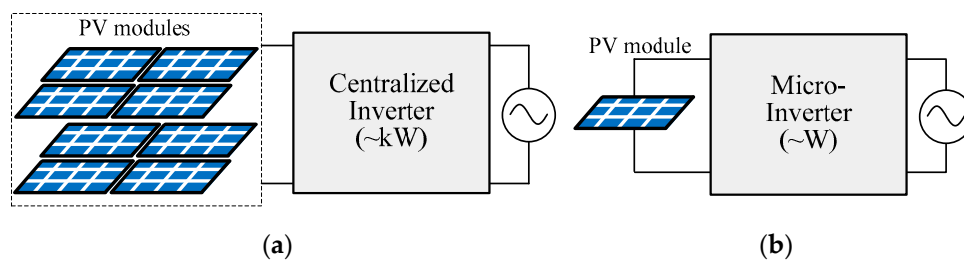

Figure 1. Configuration of PV power generative system. (**a**) Centralized inverter and (**b**) micro-inverter.

On the other hand, the micro-inverters require a long lifetime and the PV panels, likewise, are ideally maintenance-free. However, the electrolytic capacitor may decay over the lifetime of the converter. In particular, bulky electrolytic capacitor is necessary on the single-phase AC system in order to compensate the double-line frequency power ripple. In order to solve this problem, the micro-inverter with the active power decoupling circuit is considered in this paper.

Note that the micro-inverter systems are the distributed power supply, and each power converter transfers the generative power to the single-phase AC grid independently. Typically the all-converter operation is regulated by the Power Line Connection (PLC), and it is easy to get some information such as the power generation status. In this system, the micro-inverters are operated independently, and each power converters does not interfere with each other by the circuit operation.

Figure 2 shows the circuit configuration of the DC to single-phase AC converter which consists of LLC resonant converter and an active power decoupling circuit. The active power decoupling circuit compensates the double-line frequency power ripple due to the single-phase grid by the small

capacitor [13]. The LLC resonant converter transfers the input power to the secondary side. After that, the boost-up of the DC link voltage and the power decoupling operation are achieved by the active power decoupling circuit. Finally, the grid connection is achieved by the Current Source Inverter (CSI). Note that the reverse-blocking diode is not necessary on CSI because the free-wheeling mode is implemented on the active power decoupling circuit.
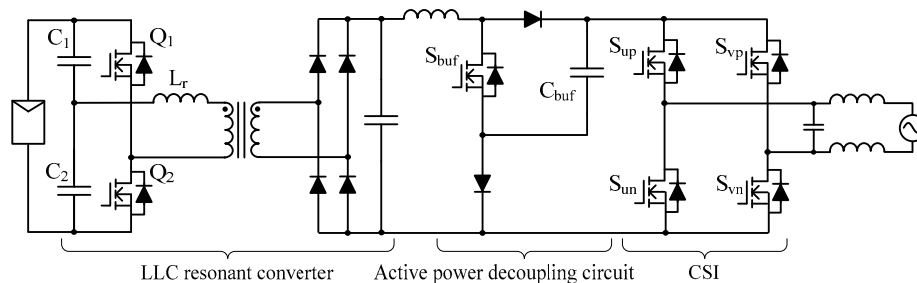

Figure 2. Circuit configuration of DC to Single-phase AC converter using LLC resonant converter.

3. Operation Principle of Active Power Decoupling Circuit

Figure 3 shows the principle of the power decoupling between the DC and single-phase AC sides [14]. In this system, the sinusoidal inverter output current is generated by the power converter in order to transfer the power to the single-phase AC grid. In this case, the single-phase grid voltage and the inverter output current are expressed as

$$v_{out} = V_{acp} \sin \omega t \tag{1}$$

$$i_{out} = I_{acp} \sin \omega t \tag{2}$$

where V_{acp} is the peak grid voltage and I_{acp} is the peak inverter current of the single-phase AC grid. When both the output voltage and the current waveforms are sinusoidal, the instantaneous output power pout is expressed as

$$p_{out} = v_{out}i_{out} = \frac{V_{acp}I_{acp}}{2}(1 - \cos 2wt) \tag{3}$$

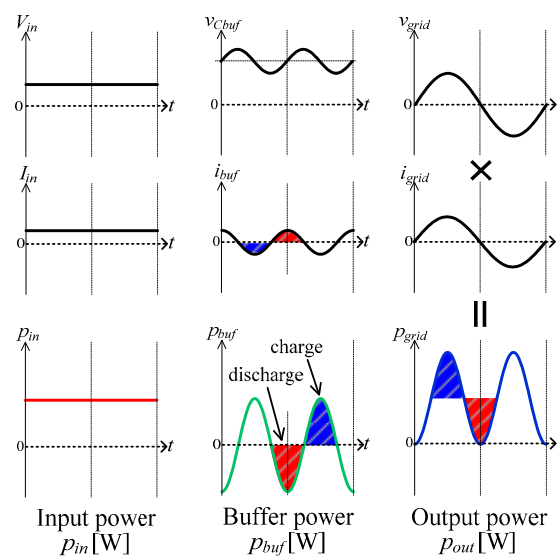from (3), the power ripple that contains double-line frequency of the power grid, appears at DC link.

Figure 3. Principle of power decoupling between DC and single-phase AC.

In order to absorb the power ripple, the instantaneous power p_{buf} should be controlled by

$$p_{buf} = \frac{V_{acp}I_{acp}}{2} \cos 2\omega t \tag{4}$$

where the polarity of p_{buf} is defined as positive when the energy C_{fc} discharges. Due to the power decoupling capability, the input power is matched to the average output power of the single-phase AC. Therefore, the relationship between the input and output power is obtained as

$$p_{in} = \frac{1}{2}V_{acp}I_{acp} = V_{PV}I_{PV} \tag{5}$$

where V_{pv} is the PV input voltage and I_{pv} is the PV input current.

Figure 4 shows the operation mode of the active power decoupling circuit when the grid voltage is the positive period. This converter has the charge mode and discharge mode of the small buffer capacitor C_{buf} in order to regulate the capacitor voltage. In order to obtain the buffer power as per Equation (4), the capacitor voltage is actively fluctuated at the twice of the grid frequency such as Figure 3.
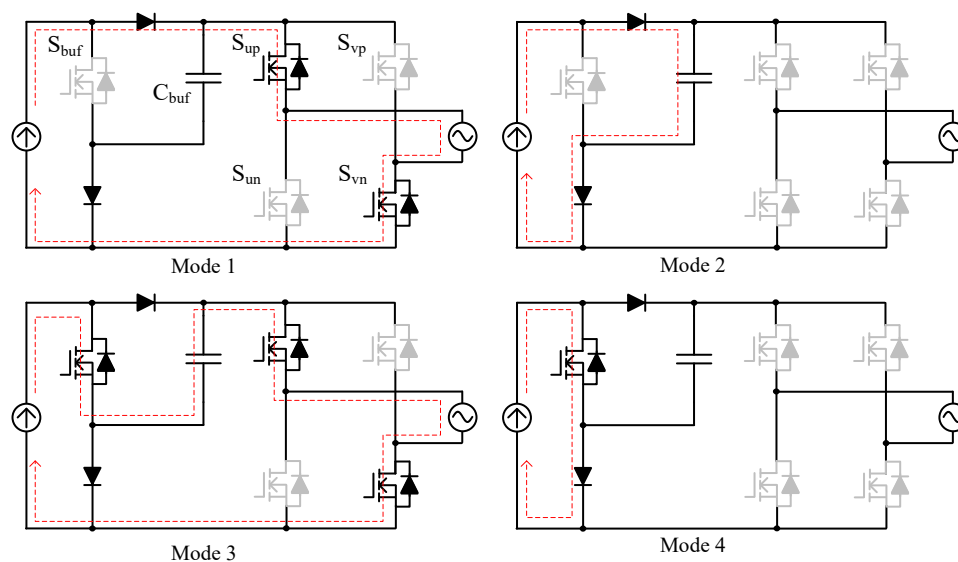

Figure 4. Operation mode of active power decoupling circuit.

The operation of the active power decoupling circuit cooperates with the CSI; this achieves both power decoupling and power transmission to the single-phase AC grid. In mode 1, the switch S_{buf} is turned on, and the input power is transferred to the single-phase AC grid. In mode 2, all the switches are turned off, and the buffer capacitor is charged. In mode 3, the buffer capacitor is discharged through the S_{buf} and CSI. Finally, mode 4 is the free-wheeling mode. The buffer capacitor voltage is regulated to adjust the duty command for modes 2 and 3 on the one period of the triangle carrier.

4. Operation Mode of LLC Resonant Converter

Figure 5 shows the operation mode, and the Figure 6 shows the key waveforms of the LLC resonant converter. In this circuit, the series resonance of C_1, C_2, and L_{res} is utilized for soft switching. The LLC converter regulates the input voltage of the active power decoupling circuit. The detail of the operation mode is as follows.
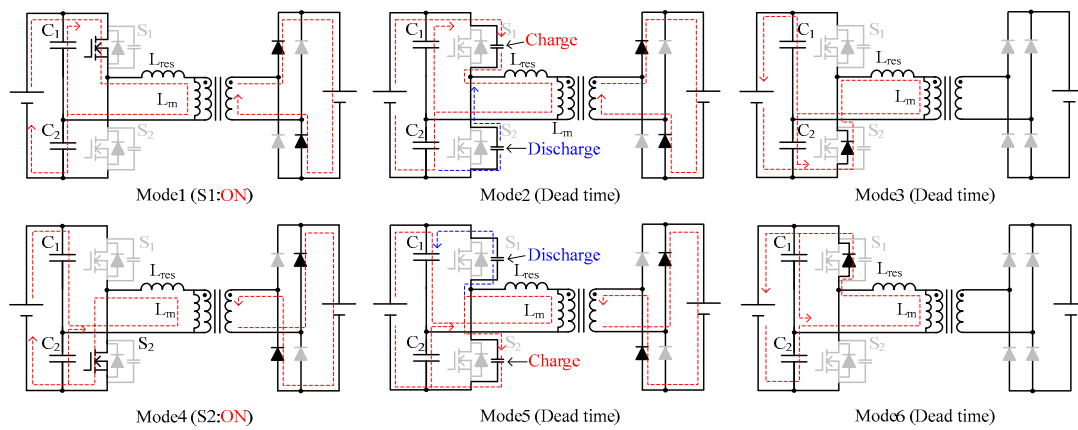
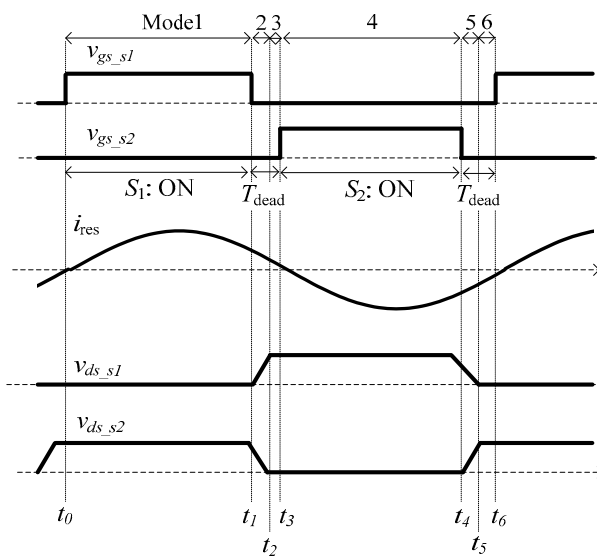**Figure 5.** Operation mode of LLC resonant converter.

Figure 6. Key waveforms of LLC resonant converter.

Mode 1 [t_0-t_1]: S_1 is turned-on and half of the PV input voltage is applied to the transformer. In this mode, C_1, C_2, and L_{res} resonate, and the resonance current occurs.

Mode 2 [t_1-t_2]: S_1 is turned-off and the dead-time period is started. At this mode, S_1 achieves ZCS turned off. In mode 2, the parasitic capacitor C_{ds1} is quickly charged. On the other hand, the parasitic capacitor C_{ds2} is discharged owing to the negative resonant current. C_{ds2} is fully discharged in this mode, and mode 3 is started.

Mode 3 [t_2-t_3]: This mode is still dead-time, and the parasitic diode of S_2 conducts. Discharge of C_{ds2} should be completed during Mode2 and 3 for ZVS of S_2.

Mode 4 [t_3-t_4]: S_2 is turned on with ZVS when C_{ds2} is already discharged. In this mode, C_1, C_2, and L_{res} resonate as mode 1, and the resonant current occurs.

Mode 5 [t_4-t_5]: S_2 is turned off, and the dead-time period is started. At this mode, S_2 achieves ZCS turned-off. In mode5, the parasitic capacitor C_{ds1} is quickly charged. On the other hand, the parasitic capacitor C_{ds1} is discharged owing to the negative resonant current.

Mode 6 [t_5-t_6]: This mode is still dead-time, and the parasitic diode of S_1 conducts. Discharge of C_{ds1} should be completed during modes 5 and 6 for ZVS of S_1.

5. Experimental Result with Fundamental Operation

5.1. Active Power Decoupling Circuit and CSI

Table 1 shows the experimental parameters. Figure 7 shows the experimental result. Note that the output power is 300 W, the switching frequency is 20 kHz, the buffer capacitor is 44 μF, and the grid voltage is 200 V_{rms}.

Table 1. Experimental parameters.

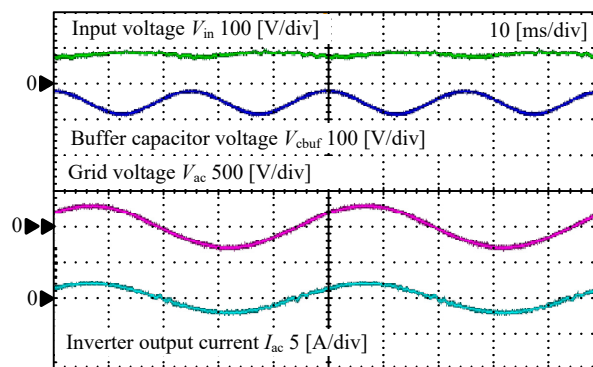| Symbol	Quantity	Value
V_{in}	Input Voltage	90 V
P_{in}	Input Power	300 W
C_{buf}	Buffer Capacitor	44 μF
V_{ac}	Grid Voltage	200 V_{rms}
f_{ac}	Grid frequency	50 Hz
f_{sw}	Switching frequency	20 kHz

Figure 7. Experimental result of active power decoupling circuit and current source inverter (CSI).

According to Figure 7, the constant DC voltage and the sinusoidal inverter output current with the low THD are obtained. In addition, it is obtained that the buffer capacitor voltage is fluctuated by the double-line frequency by the power decoupling control. However, the low frequency component is still remaining on the input voltage. This is because the mismatch is occurring during the compensation value and the actual power ripple component. The compensation value for the power decoupling is obtained from the input power. However, the input power is included the conversion loss, which means the error between the compensation power and the actual output power occurs. This problem is solved by changing the calculation process of the compensation value to use the output power condition.

5.2. LLC Resonant Converter

Table 2 shows the experimental parameters and Figure 8 shows the experimental result. Note that the resonant frequency is designed to 205 kHz, and the switching frequency is set to below the resonant frequency as Table 2. In addition, the gate signals of S_1 and S_2 is provided by the 50% of duty signals from the controller. According to Figure 8, the sinusoidal resonant current is obtained by the series resonance.

Table 2. Experimental parameters.

| Symbol	Quantity	Value
V_{in}	Input Voltage	40 V
V_{out}	Output Voltage	80 V
f_{sw}	Switching frequency	200 kHz
L_m	Magnetizing inductance	25 μH
L_{res}	Resonant inductance	400 nH
C_1, C_2	Resonant capacitance	750 nF
C_{dc}	DC capacitance	15 μF
C_j	Junction capacitance	500 pF
C_{oss}	Output capacitance	1500 pF
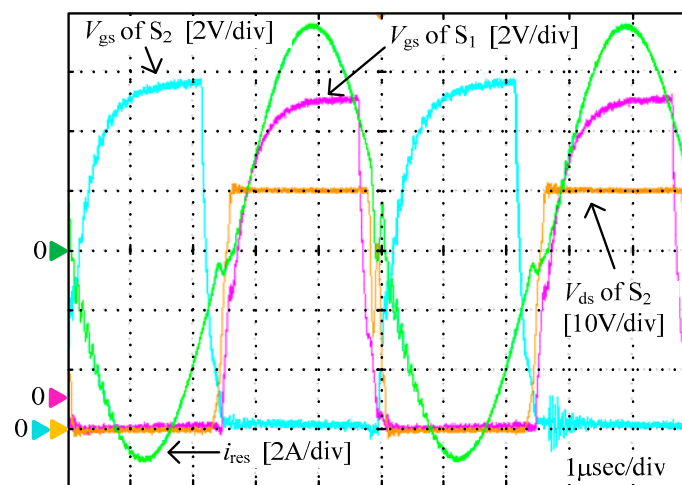
Figure 8. Switching waveforms.

Figure 9 shows the efficiency characteristics and the loss analysis result of the LLC resonant converter. According to Figure 9, 94.3% of the maximum efficiency is obtained when the output power is 100 W. In order to improve the conversion efficiency, the utilization of the synchronous rectifier is simple solution. On the other hand, the reduction of the transformer losses is important for the high switching frequency DC/DC converter because the copper loss becomes largely due to the skin effect and the proximity effect [15].
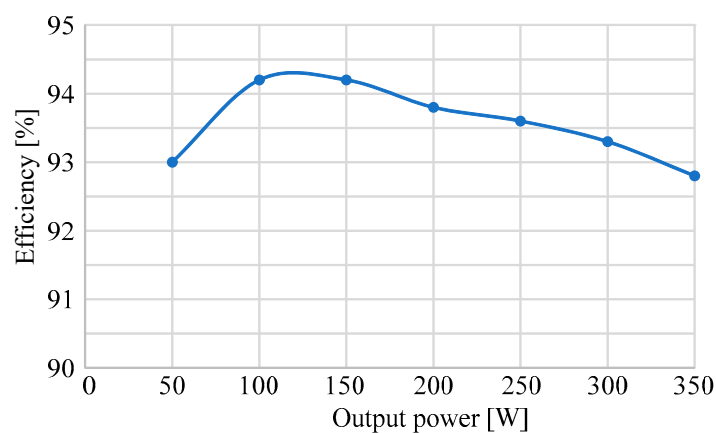
Figure 9. Efficiency curve.

6. Evaluation of Conversion Efficiency Using Different Litz Wire

In this section, the conversion efficiency of the LLC converter is evaluated in terms of a change the transformer. The high switching frequency operation increases the transformer loss including the copper loss due to the skin effect and the proximity effect, eddy loss, and hysteresis loss. Especially the skin effect and the proximity effect reduce the effective conduction area to surface of the wiring. As the result, the alternative wire resistance becomes large. In order to avoid this problem, the litz wire is usually used. In this paper, the two types of transformer are evaluated when the number of strands is changed.

Figure 10 shows the overview of the transformer, and Tables 3 and 4 show the parameter of the two transformers. Note that the air gap is not provided on this transformer in order to eliminate the leakage flax from the air gap, and the ferrite core with low eddy current loss is selected for the high switching frequency operation. The difference between two transformers is only number of strands, with transformer 2 having many strands on the wiring.
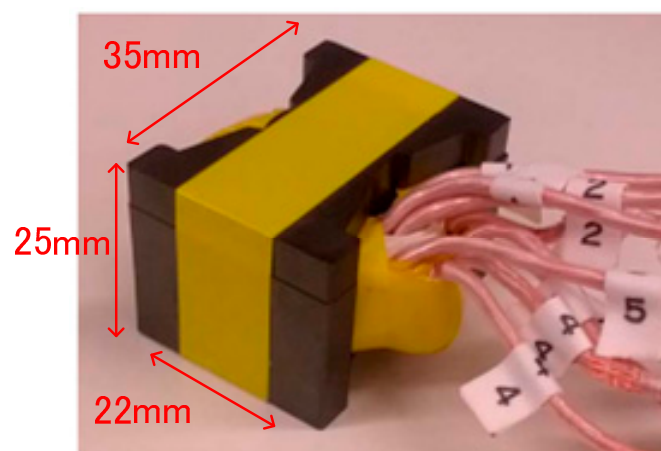

Figure 10. Overview of high frequency transformer.

Table 3. Parameters of transformer 1.

Symbol	Quantity	Value
N_1	Primary side number of turns	2
N_2	Secondary side number of turns	8
-	Litz wire specification	150/ϕ0.1
-	Current density	4 A/mm^2
-	Core material	Ferrite (PQ)
-	Air gap	0 mm
L_m	Magnetizing inductance	21.3 μH

Table 4. Parameters of transformer 2.

Symbol	Quantity	Value
N_1	Primary side number of turns	2
N_2	Secondary side number of turns	8
-	Litz wire specification	600/ϕ0.05
-	Current density	4 A/mm^2
-	Core material	Ferrite (PQ)
-	Air gap	0 mm
L_m	Magnetizing inductance	21.5 μH

Figure 11 shows the comparison of the conversion efficiency when the number of the strands is changed. Note that the orange and blue line means the approximate curve of each plot. The switching frequency is set to 200 kHz, and the same transformer core material is used. In this experiment, the conversion efficiency of the LLC converter with difference number and diameter of strands as shown in Table 3 is compared. According to Figure 11, it is obtained that the conversion efficiency is improved by 1% when the number of strand is increased on the wiring. This is because the increasing AC resistance due to the skin effect is suppressed, and the copper loss is reduced. Therefore, the litz wire with a lot of strands has a good performance in order to improve the conversion efficiency for the high switching frequency converter. Note that Figure 12 shows the comparison of the conversion efficiency when the switching frequency is changed. Note that the orange and blue lines represent the approximate curve of each plot. According to Figure 12, it is obtained that the improvement rate of the conversion efficiency is increased at 200 kHz. From this result, the number of strands should be chosen accordingly because it depends on the switching frequency.
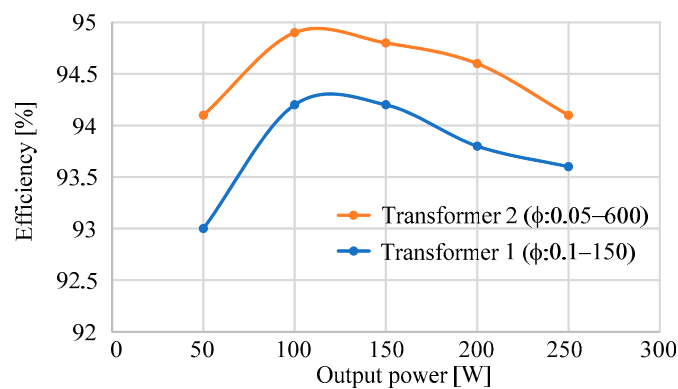

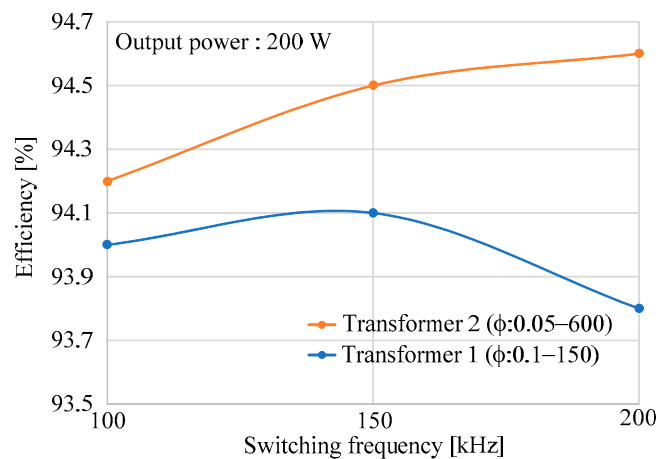**Figure 11.** Comparison of conversion efficiency when number of strands is changed on wiring.

Figure 12. Comparison of conversion efficiency when switching frequency is changed.

7. Conclusions

In this paper, a DC–single-phase AC power converter with an LLC resonant converter is presented for a photovoltaic (PV) micro-inverter application. This converter consists of the LLC resonant converter, the active power decoupling circuit, and the CSI. In addition, the conversion efficiency of the LLC converter is evaluated when the number of strands is changed. Through the experimental result, it was obtained that the double-line frequency ripple is compensated by the small capacitor using an active power decoupling circuit. Finally, the conversion efficiency of the LLC converter is improved by 1% when the litz wire have a lot of strands.

In the future work, the optimal design of the high frequency transformer will be considered. In particular, the optimal number of the strand should be considered in order to minimize the transformer loss, and it depends on the switching frequency. Therefore, the relationship between the number of strands and the switching frequency will be analyzed. Finally, the optimal transformer design focusing on the minimum transformer losses will be demonstrated based on the loss analysis.

References

1. Lee, H.Y.; Yun, J.J. Quasi-Resonant Voltage Doubler with Snubber Capacitor for Boost Half-Bridge DC–DC Converter in Photovoltaic Micro-Inverter. *IEEE Trans. Power Electron.* **2019**, *34*, 8377–8388. [CrossRef]

2. Gautam, A.R.; Fulwani, D. Adaptive SMC for the Second-Order Harmonic Ripple Mitigation: A Solution for the Micro-Inverter Applications. *IEEE Trans. Power Electron.* **2019**, *34*, 8254–8264. [CrossRef]

3. Liao, C.Y.; Lin, W.S.; Chen, Y.M.; Chou, C.Y. A PV Micro-inverter with PV Current Decoupling Strategy. *IEEE Trans. Power Electron.* **2019**, *32*, 6544–6557. [CrossRef]

4. Leuenberger, D.; Biela, J. PV-Module-Integrated AC Inverters (AC Modules) with Subpanel MPP Tracking. *IEEE Trans. Power Electron.* **2017**, *32*, 6105–6118. [CrossRef]

5. Sun, W.; Xing, Y.; Wu, H.; Ding, J. Modified High-Efficiency LLC Converters with Two Split Resonant Branches for Wide Input-Voltage Range Applications. *IEEE Trans. Power Electron.* **2018**, *33*, 7867–7879. [CrossRef]

6. Qian, T.; Qian, C. An Adaptive Frequency Optimization Scheme for LLC Converter with Adjustable Energy Transferring Time. *IEEE Trans. Power Electron.* **2019**, *34*, 2018–2024. [CrossRef]

7. Yamamoto, T.; Konno, Y.; Sugimura, K.; Sato, T.; Bu, Y.; Mizuno, T. Loss Reduction of LLC Resonant Converter using Magnetocoated Wire. *IEEJ J. Ind. Appl.* **2019**, *8*, 51–56. [CrossRef]

8. Yamamoto, T.; Bu, Y.; Mizuno, T.; Yamaguchi, Y.; Kano, T. Loss Reduction of Transformer for LLC Resonant Converter Using a Magnetoplated Wire. *IEEJ J. Ind. Appl.* **2018**, *7*, 43–48. [CrossRef]

9. Kimura, S.; Nanamori, K.; Kawakami, T.; Imaoka, J.; Yamamoto, M. Allowable Power Analysis and Comparison of High Power Density DC-DC Converters with Integrated Magnetic Components. *IEEJ J. Ind. Appl.* **2017**, *6*, 463–472. [CrossRef]

10. Liu, B.; Liu, Z.; Liu, J.; Wu, T.; Wang, S. A feedforward control based power decoupling scheme for voltage-controlled grid-tied inverters. In Proceedings of the IEEE Applied Power Electronics Conference and Exposition, Long Beach, CA, USA, 20–24 March 2016; pp. 3328–3332.

11. Liu, X.; Dong, D.; Harfman-Todorovic, M.; Garaces, L. A PV Micro-inverter With PV Current Decoupling Strategy. In Proceedings of the IEEE Applied Power Electronics Conference and Exposition, Long Beach, CA, USA, 20–24 March 2016; pp. 3403–3408.

12. Roßkopf, A.; Bär, E.; Joffe, C. Influence of Inner Skin-and Proximity Effects on Conduction in Litz Wires. *IEEE Trans. Power Electron.* **2014**, *29*, 5454–5461. [CrossRef]

13. Ohnuma, Y.; Orikawa, K.; Itoh, J.I. A Single-Phase Current Source PV Inverter with Power Decoupling Capability Using an Active Buffer. In Proceedings of the IEEE Energy Conversion Congress and Exposition, Denver, CO, USA, 15–19 September 2013; pp. 3094–3101.

14. Watanabe, H.; Itoh, J.I. Zero Voltage Switching Scheme for Flyback Converter to Ensure Compatibility with Active Power Decoupling Capability. In Proceedings of the International Power Electronics Conference, Niigata, Japan, 20–24 May 2018; pp. 896–903.
15. Hurley, W.G.; Wolfle, W.H.; Breslin, J.G. Optimized Transformer Design: Inclusive of High-Frequency Effects. *IEEE Trans. Power Electron.* **1998**, *13*, 651–659. [CrossRef]